

## <sup>73</sup>Ge-Nuclear Magnetic Resonance/Nuclear Quadrupole Resonance Investigation of Magnetic Properties of URhGe

Hisashi Kotegawa<sup>1\*</sup>, Kenta Fukumoto<sup>1</sup>, Toshihiro Toyama<sup>1</sup>, Hideki Tou<sup>1</sup>,  
Hisatomo Harima<sup>1</sup>, Atsushi Harada<sup>2</sup>, Yoshio Kitaoka<sup>2</sup>, Yoshinori Haga<sup>3</sup>,  
Etsuji Yamamoto<sup>3</sup>, Yoshichika Ōnuki<sup>3,4</sup>, Kohei M. Itoh<sup>5</sup>, and Eugene E. Haller<sup>6</sup>

<sup>1</sup>Department of Physics, Kobe University, Kobe 657-8501, Japan

<sup>2</sup>Graduate School of Engineering Science, Osaka University, Osaka 560-8531, Japan

<sup>3</sup>ASRC, JAEA, Tokai, Ibaraki 319-1195, Japan

<sup>4</sup>Faculty of Science, University of the Ryukyus, Nishihara, Okinawa 903-0213, Japan

<sup>5</sup>School of Fundamental Science and Technology, Keio University, Yokohama 223-8522, Japan

<sup>6</sup>Department of Materials Science and Engineering, University of California at Berkeley  
and Lawrence Berkeley National Laboratory, Berkeley, CA 94720, U.S.A.

(Received January 20, 2015; accepted March 13, 2015; published online April 27, 2015)

We report on the <sup>73</sup>Ge-nuclear magnetic resonance (NMR)/nuclear quadrupole resonance (NQR) results for the ferromagnetic (FM) superconductor URhGe. The magnitude and direction of the internal field,  $H_{\text{int}}$ , and the parameters of the electric field gradient at the Ge site were determined experimentally. By using powdered polycrystalline samples oriented by different methods, the field dependences of NMR shift and nuclear spin relaxation rates for  $H_0 \parallel c$  (easy axis) and  $H_0 \parallel b$  were obtained. From the NMR shifts for  $H_0 \parallel b$ , we confirmed a gradual suppression of the Curie temperature and observed a phase separation near the spin reorientation. The observation of the phase separation gives microscopic evidence that the spin reorientation under  $H_0 \parallel b$  is of first order at low temperatures. The nuclear spin-lattice relaxation rate  $1/T_1$  indicates that the magnetic fluctuations are suppressed for  $H_0 \parallel c$ , whereas the fluctuations remain strongly for  $H_0 \parallel b$ . The enhancements of both  $1/T_1T$  and the nuclear spin-spin relaxation rate  $1/T_2$  for  $H_0 \parallel b$  toward the spin reorientation field suggest that the field-induced superconductivity in URhGe emerges under the magnetic fluctuations along the  $b$ - and  $c$ -axes.

### 1. Introduction

The intimate interplay between superconductivity and magnetism has been intensively investigated in many unconventional superconductors such as cuprates, heavy fermion systems, organic superconductors, and Fe-pnictides. Superconductivity is realized in various situations; however, among them, novel superconductivity coexisting with ferromagnetism emerges only in uranium compounds such as UGe<sub>2</sub>, URhGe, UCoGe, and UIr.<sup>1-4</sup> The first three compounds have several similarities; for instance, they have crystallographically similar U-zigzag chains, and each magnetic anisotropy is of Ising type. On the other hand, quantitative differences appear in some aspects. Superconductivity in URhGe occurs at  $T_{\text{sc}} = 0.25$  K well below the Curie temperature,  $T_{\text{Curie}}$ , of 9.5 K.<sup>2)</sup> The ordered moment of  $0.42 \mu_{\text{B}}/\text{U}$  lies along the  $c$ -axis.<sup>2)</sup> These values are different among the three compounds:  $T_{\text{sc}} = 0.6$  K,  $T_{\text{Curie}} = 2.8$  K, and  $0.03 \mu_{\text{B}}/\text{U}$  for UCoGe,<sup>3)</sup> and  $T_{\text{sc}} = 0.7$  K,  $T_{\text{Curie}} \sim 30$  K, and  $0.9 \mu_{\text{B}}/\text{U}$  for UGe<sub>2</sub> (at 1.2 GPa).<sup>1)</sup> A comparison among these compounds is essential for understanding what is an important factor in ferromagnetic (FM) superconductors.

Another notable phenomenon is field-induced superconductivity, which is observed remarkably in URhGe when the magnetic field is applied along the  $b$ -axis.<sup>5)</sup> Superconductivity disappears once by applying a magnetic field of more than 2 T, but the system reenters the superconducting (SC) phase above 8 T. Torque measurements have suggested that the spin reorientation from the  $c$ -axis to the  $b$ -axis occurs at the spin reorientation field,  $H_{\text{R}} \sim 12$  T. In UCoGe and UGe<sub>2</sub>, SC phases are not separated, but unusual field dependences of the upper critical field  $H_{c2}$  are observed.<sup>6,7)</sup>

Nuclear magnetic resonance (NMR) and nuclear quadrupole resonance (NQR) measurements have contributed to promoting an understanding of the FM superconductors. In UGe<sub>2</sub> and UCoGe, various properties such as the microscopic coexistence of superconductivity and ferromagnetism, microscopic states of the phase boundary, a character of the magnetic fluctuations, and spin susceptibility have been confirmed and discussed.<sup>8-15)</sup> However, no NMR/NQR experimental data have been reported on URhGe. In this paper, we report on <sup>73</sup>Ge-NMR/NQR results for URhGe to reveal its magnetic properties. URhGe belongs to the  $Pnma$  space group, possessing one Ge site, and the local symmetry at the Ge site is expressed by  $[.m.]$ .

### 2. Experimental Procedure

A polycrystalline sample was prepared using enriched <sup>73</sup>Ge. Unfortunately, the sample quality was not sufficient for inducing superconductivity; the residual resistivity ratio (RRR) was about 4. In this paper, we focus on the magnetic properties of URhGe, which are not considered to be very sensitive to the sample quality, because the spin reorientation has been observed at similar magnetic fields for the samples whose RRR values range from 12 to 40.<sup>16)</sup> NQR measurement was performed using the powdered sample, and the sample was oriented along both  $H_0 \parallel c$  and  $H_0 \parallel b$  for NMR measurements. The nuclear spin-lattice relaxation time  $T_1$  was measured at the  $\pm 7/2 \leftrightarrow \pm 9/2$  transition for the paramagnetic (PM) state, the  $+1/2 \leftrightarrow +3/2$  transition for the FM state at zero field, and at the central ( $-1/2 \leftrightarrow +1/2$ ) transition for the NMR measurements. Each recovery curve was fitted to the theoretical function corresponding to the transition to estimate  $T_1$ . The nuclear spin-spin relaxation time  $T_2$  was measured at the central transition for  $H_0 \parallel b$ ,

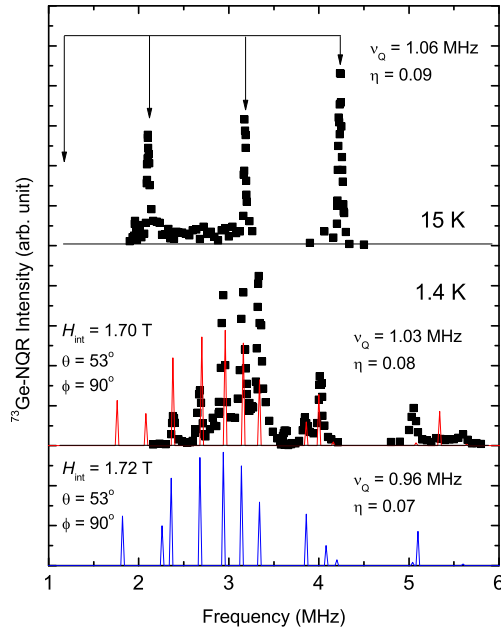


**Fig. 1.** (Color online)  $^{73}\text{Ge}$ -NQR spectra measured at zero field in the PM and FM states. In the PM state, three transitions were observed among four transitions for  $I = 9/2$ . The complicated spectrum in the FM state can be almost reproduced using the parameters described in the figure. We show two sets of parameters, but it was difficult to determine which set of parameters is better.

and the decay curves were fitted to the single exponential function.

### 3. Experimental Results and Discussion

#### 3.1 NQR/NMR spectral analysis

Figure 1 shows  $^{73}\text{Ge}$ -NQR spectra measured at zero field. In the PM phase at 15 K, three peaks are observed in the frequency range from 2 to 4.5 MHz. Each peak corresponds to  $\pm 3/2 \leftrightarrow \pm 5/2$  ( $\sim 2.1$  MHz),  $\pm 5/2 \leftrightarrow \pm 7/2$  ( $\sim 3.2$  MHz), and  $\pm 7/2 \leftrightarrow \pm 9/2$  ( $\sim 4.2$  MHz) transitions. These resonance frequencies provide the quadrupole frequency  $\nu_Q = 1.06$  MHz and the asymmetry parameter  $\eta = 0.09$ . In the ordered state at 1.4 K, the emergence of the internal field modifies the spectral shape. The spectrum is complicated, but it can be almost reproduced by simulations using the following parameters: (red curve:  $H_{\text{int}} = 1.70$  T,  $\theta = 53^\circ$ ,  $\phi = 90^\circ$ ,  $\nu_Q = 1.03$  MHz, and  $\eta = 0.08$ ), or (blue curve:  $H_{\text{int}} = 1.72$  T,  $\theta = 53^\circ$ ,  $\phi = 90^\circ$ ,  $\nu_Q = 0.96$  MHz, and  $\eta = 0.07$ ). Here,  $H_{\text{int}}$  is the magnitude of the internal field at the Ge site, and  $\theta$  and  $\phi$  are respectively the angles between the principal axes of the electric field gradient (EFG) and the effective field at the Ge site,  $H_{\text{eff}}$ , which is equal to  $H_{\text{int}}$  under zero external field. It was difficult to determine which set of parameters is better between the two sets. The red curve does not reproduce the signal at approximately 5 MHz, but  $\nu_Q$  and  $\eta$  are consistent with those obtained from the NMR spectrum.

Figures 2(a) and 2(b) show  $^{73}\text{Ge}$ -NMR spectra measured under external magnetic fields. The spectrum in Fig. 2(a) was obtained after applying a mechanical shock to the powdered sample at low temperatures so as to orient the magnetic easy axis of the crystal, that is, the  $c$ -axis toward the magnetic field. The spectrum consists of nine well-separated peaks, which ensure a high degree of orientation. The spectrum can be reproduced by the parameters  $H_{\text{eff}} = 10.69$  T,  $\theta = 75.5^\circ$ ,

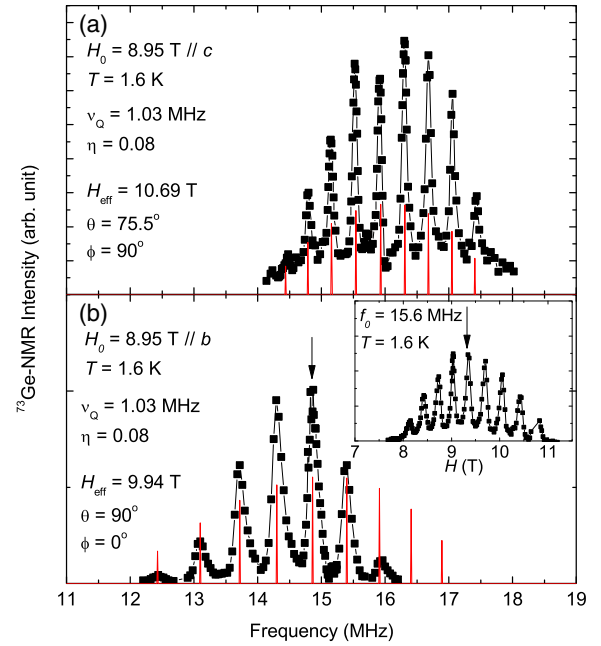


**Fig. 2.** (Color online)  $^{73}\text{Ge}$ -NMR spectra of URhGe for the samples oriented along (a)  $H_0 \parallel c$  and (b)  $H_0 \parallel b$ . At 8.95 T, each spectrum was observed in different frequency ranges. The inset shows a field-swept spectrum with a fixed frequency for  $H_0 \parallel b$ . The central transition is observed at  $\sim 9.4$  T, which corresponds to the peak at  $\sim 14.8$  MHz in the frequency-swept spectrum as shown by arrows. In the frequency-swept spectrum, the measurement above 16.2 MHz has not been performed. The sharp peaks in all the spectra ensure the high degree of orientation.

$\phi = 90^\circ$ ,  $\nu_Q = 1.03$  MHz, and  $\eta = 0.08$ . Here,  $H_{\text{eff}}$  is an effective field at the Ge site, which is a vector sum of the external field  $H_0$  and  $H_{\text{int}}$ , that is,  $H_{\text{eff}} = H_0 + H_{\text{int}}$ .

A first-principles calculation showed that the direction of the first principal axis of the EFG,  $V_{zz}$ , is tilted somewhat from the  $a$ -axis to the  $c$ -axis, and the second principal axis lies along the  $b$ -axis;<sup>17)</sup> thus, we considered that  $V_{zz}$  ( $\theta = 0^\circ$ ) lies in the  $ac$  plane and the second principal axis ( $\theta = 90^\circ$ ,  $\phi = 0^\circ$ ) lies along the  $b$ -axis, as shown in Fig. 3. The angles of  $\phi = 90^\circ$  obtained in Figs. 1 and 2(a) indicate that  $H_{\text{int}}$  and  $H_{\text{eff}}$  are in the  $ac$  plane. From the zero-field spectrum, the angle between  $H_{\text{int}}$  and  $V_{zz}$  is deduced experimentally as  $53^\circ$ , and the angle between  $H_{\text{eff}}$  and  $V_{zz}$  is determined as  $75.5^\circ$  from the NMR spectrum. Next, we assumed that the direction of  $H_{\text{int}}$  is independent of the external field applied along the  $c$ -axis. This is consistent with the assumption that the hyperfine coupling tensor is independent of  $H_0$ , and the magnetic moment is directed to the  $c$ -axis both at zero field and under  $H_0 \parallel c$ . Then, the angle between  $H_{\text{eff}}$  and  $H_{\text{int}}$  is estimated as  $75.5^\circ - 53^\circ = 22.5^\circ$ . By using this angle and the relation  $H_{\text{eff}} = H_0 + H_{\text{int}}$ , the internal field  $H_{\text{int}} = 1.92$  T under  $H_0 = 8.95$  T can be estimated. Similarly, the angle between  $H_{\text{int}}$  and  $H_0$ , which is along the  $c$ -axis, can be determined as  $27.2^\circ$ . Consequently, we evaluated that  $V_{zz}$  is tilted by  $9.8^\circ$  from the  $a$ -axis, as shown in Fig. 3.

On the other hand, the spectra in Fig. 2(b) and its inset were obtained by a method different from that shown in Fig. 2(a). The sample was fixed in paraffin at  $\sim 60^\circ\text{C}$  under 10 T; thus, the crystals were oriented along the easy axis at high temperatures, which was the  $b$ -axis. As shown in Figs. 2(a) and 2(b), the two spectra measured in the same magnetic field and temperature are observed in different

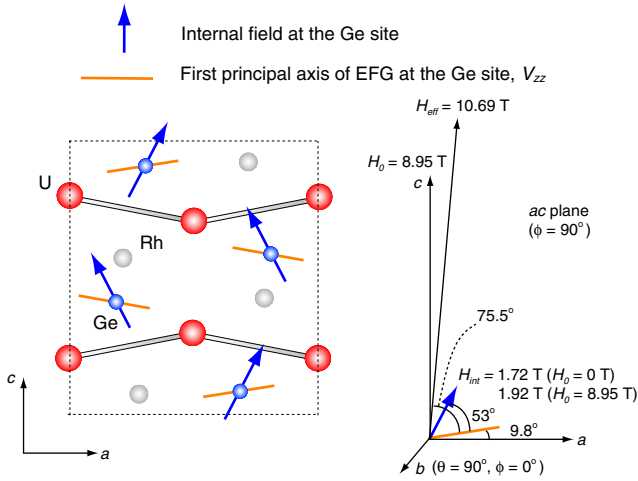


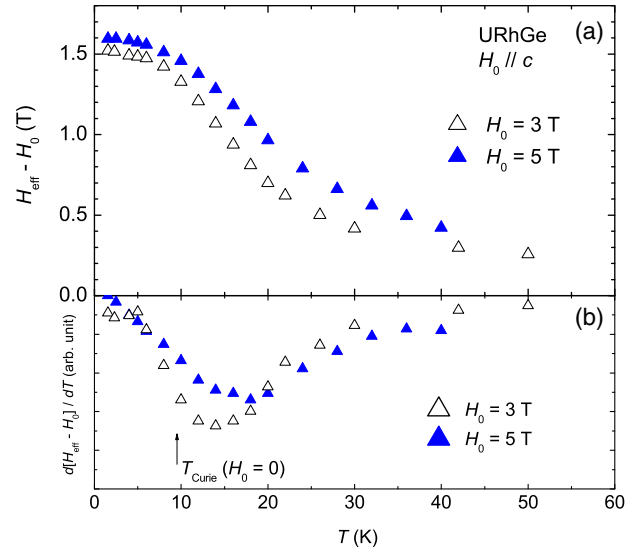
**Fig. 3.** (Color online) Relationships among the crystal axes, the principal axes of the EFG, and each magnetic field,  $H_{\text{int}}$  and  $H_{\text{eff}}$ . It is assumed that  $V_{zz}$  ( $\theta = 0^\circ$ ) lies in the  $ac$  plane and the second principal axis ( $\theta = 90^\circ$ ,  $\phi = 0^\circ$ ) lies along the  $b$ -axis from the first-principles calculation. The  $H_{\text{int}}$  at the Ge site is tilted slightly from the  $c$ -axis. This is expected to originate from the anisotropy of the hyperfine coupling constants.

frequency ranges. The inset shows a field-swept spectrum in which a central transition was observed at  $\sim 9.4$  T. In the frequency-swept spectrum, this transition corresponds to the peak at  $\sim 14.8$  MHz, which is lower than the central transition of  $\sim 15.9$  MHz for  $H_0 \parallel c$ , indicating that the internal field along  $H_0$  is much smaller than the case of  $H_0 \parallel c$ . The spectrum in Fig. 2(b) is reproduced by  $\theta = 90^\circ$  and  $\phi = 0^\circ$ , which are the angles obtained when  $H_{\text{eff}}$  is parallel to the  $b$ -axis. Actually, the directions of  $H_0$  and  $H_{\text{eff}}$  are slightly different owing to the presence of  $H_{\text{int}}$ , but this contribution is expected to be small because of  $H_0 \gg H_{\text{int}}$ . Therefore, the simulation indicates that the crystals are oriented along  $H_0 \parallel b$ . The orientation along  $H_0 \parallel b$  is also confirmed by a signature of the field-induced spin reorientation, as described later.

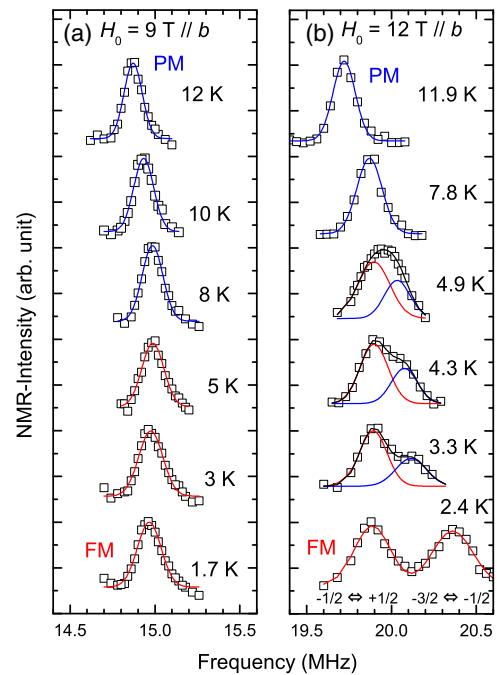
### 3.2 Temperature dependences of the NMR shifts

Figure 4(a) shows the temperature dependence of NMR shift defined as  $H_{\text{eff}} - H_0$  for  $H_0 \parallel c$  (easy axis). The increase in the shift at  $\sim 10$ – $20$  K originates from the development of the magnetization along the  $c$ -axis,  $M_c$ . The shifts at 1.6 K under 3, 5, and  $\sim 9$  T and the magnetization data<sup>18)</sup> gave a hyperfine coupling constant along the  $c$ -axis as  $A^c \sim 3.24$  T/ $\mu_B$ . Here,  $A^c$  is defined as  $H_{\text{eff}} - H_0 = A^c M_c$ . The temperature derivatives of the shifts show peaks, which depend on  $H_0$ , as shown in Fig. 4(b). This temperature corresponding to the increase in the magnetization is estimated to be  $\sim 14$  K at  $H_0 = 3$  T and  $\sim 18$  K at  $H_0 = 5$  T. These are apparently higher than  $T_{\text{Curie}} = 9.5$  K at zero field, indicating that the transition is a crossover under the magnetic field along the easy axis.

Figures 5(a) and 5(b) show the NMR spectra for the central transition at several temperatures for  $H_0 \parallel b$ . At  $H_0 = 9$  T, the peak position shifts to the higher frequency with temperature decreasing to  $\sim 8$  K, and then returns to the lower frequency slightly. All the spectra are reproduced by a single Gaussian function. The temperature dependences of the NMR shift  $H_{\text{eff}} - H_0$  estimated from the resonance



**Fig. 4.** (Color online) Temperature dependence of the NMR shift  $H_{\text{eff}} - H_0$  for  $H_0 \parallel c$ . The shift increases toward low temperatures because of the development of a static moment. Their derivatives have a peak at the characteristic temperature of a crossover, which is higher than the original  $T_{\text{Curie}}$ .



**Fig. 5.** (Color online) NMR spectra of the central transitions for  $H_0 \parallel b$ . At 9 T, the peak position shifts to a higher frequency down to  $\sim 8$  K, and then returns to a lower frequency slightly. This temperature of  $\sim 8$  K corresponds to  $T_{\text{Curie}}$  under  $H_0 \parallel b$ . At 12 T, the spectrum is composed of two components at around  $T_{\text{Curie}}$ , indicating that the transition is of first order accompanied by the phase separation.

frequencies are shown in Fig. 6(a). The shift at  $H_0 = 9$  T increases with temperature decreasing to  $\sim 7$ – $8$  K, at which it has a broad maximum. This temperature corresponds to  $T_{\text{Curie}}$  under  $H_0 \parallel b$ , which decreases from the original value of  $T_{\text{Curie}} = 9.5$  K.<sup>16,18)</sup> The shifts above 9 T show that  $T_{\text{Curie}}$  decreases with further application of the magnetic field. On the other hand, the hyperfine coupling constant along the  $b$ -axis was estimated to be  $A^b \sim 3.25$  T/ $\mu_B$  from a comparison between the shift and the magnetization data in the

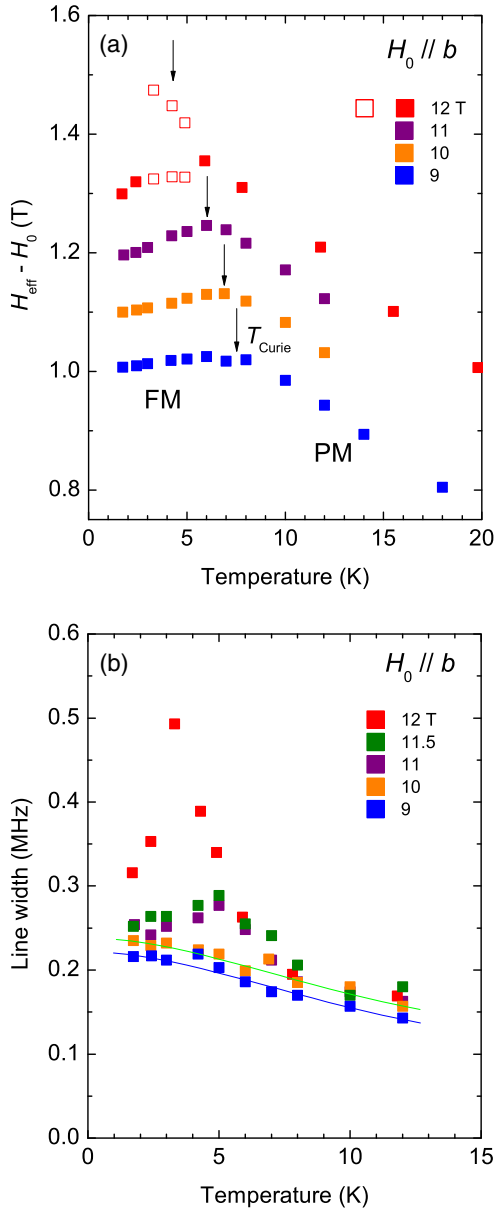


**Fig. 6.** (Color online) Temperature dependences of (a) NMR shift and (b) line width for  $H_0 \parallel b$ .  $T_{\text{Curie}}$  is determined at the peak position of the shift. At 12 T, a clear phase separation is observed in the temperature range shown by the open symbols. The shift in the PM state continues to increase toward low temperature.

PM state at 9 T.<sup>18)</sup> This value is almost the same as  $A^c = 3.24 \text{ T}/\mu_B$ .

As shown in Fig. 5(b), at  $H_0 = 12 \text{ T}$ , the behavior is similar to the case of 9 T at high temperatures, and the spectrum is reproduced by a single Gaussian function. However, the spectrum becomes broader with decreasing temperature. In particular, the spectra at 4.3 and 3.3 K are composed of two components, and each spectrum can be reproduced by a summation of two Gaussian functions as shown by red and blue curves. The overlap of two Gaussian functions gives microscopic evidence of the phase separation on a discontinuous phase transition. This is not attributed to extrinsic origins such as a misalignment of the crystals. With decreasing temperature, the component at the higher frequency shifts to the high-frequency side accompanied by a decrease in the intensity, and seems to overlap at the first

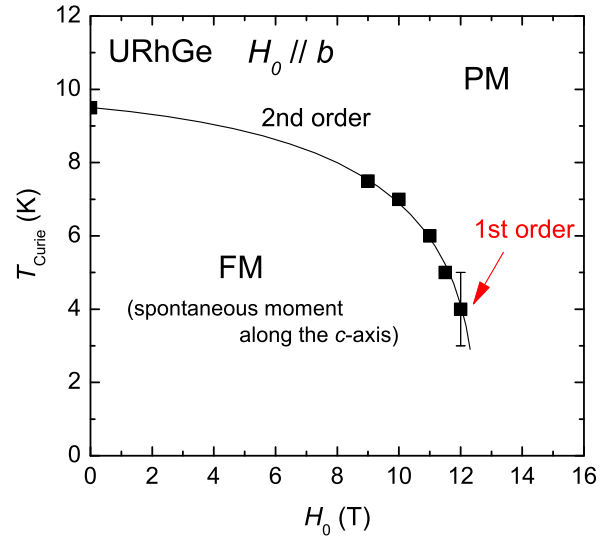


**Fig. 7.** (Color online) Magnetic field–temperature phase diagram of URhGe for  $H_0 \parallel b$ . The TCP of URhGe is expected to be located between (10 T, 7 K) and (12 T, 4 K). In the present experimental setting,  $H_R$  is roughly estimated to be  $\sim 13 \text{ T}$ .

satellite peak ( $-3/2 \leftrightarrow -1/2$  transition) at 2.4 K. We could not observe any signature of the phase separation below 2.4 K, and judged that the system is in the homogeneous FM state. The NMR shift at 12 T is shown in Fig. 6(a), where two data points are plotted at the same temperature because of the phase separation. The shift corresponding to the PM phase continues to increase toward low temperature. This tendency is consistent with the magnetization data above 12 T.<sup>18)</sup> The  $T_{\text{Curie}}$  was estimated to be  $4 \pm 1 \text{ K}$  from the NMR shift at 12 T.

Figure 6(b) shows the temperature dependence of the spectral line width under each magnetic field. Here, the line width was estimated from the full width at half maximum even for the asymmetric spectra at the phase separation region. The temperature dependences of the line width below 10 T are monotonic, suggesting that the FM transition is of second order below 10 T. At 12 T, an apparent increase in the line width is observed, and this tendency remains at 11 and 11.5 T. This may originate in the phase separation, but the broad spectra at 11 and 11.5 T are almost reproduced by a single Gaussian function. Therefore, we cannot exclude the possibility that the broadening at 11 and 11.5 T originates from the misalignment of the oriented crystals.

The magnetic field–temperature phase diagram for  $H_0 \parallel b$  is shown in Fig. 7, where  $T_{\text{Curie}}$  is determined by the NMR shift. We distinguished that the transition below 10 T is of second order, and that at 12 T is of first order accompanied by the phase separation. From our experiments, the tricritical point (TCP), at which the second-order transition changes to first-order, is roughly estimated to be located between (10 T, 7 K) and (12 T, 4 K). The presence of the TCP is consistent with other experimental and theoretical indications.<sup>5,19–21)</sup> The rough extrapolation of  $T_{\text{Curie}}$  indicates that the spin reorientation field at 0 K is present at  $H_R \sim 13 \text{ T}$  in this experimental setting. The torque measurement using a single crystal has shown that a misalignment of  $2.5^\circ$  from the  $b$ -axis to the  $c$ -axis induces the increase in  $H_R$  from  $\sim 12$  to  $\sim 13 \text{ T}$ .<sup>5)</sup> Although a direct comparison between the single crystal and

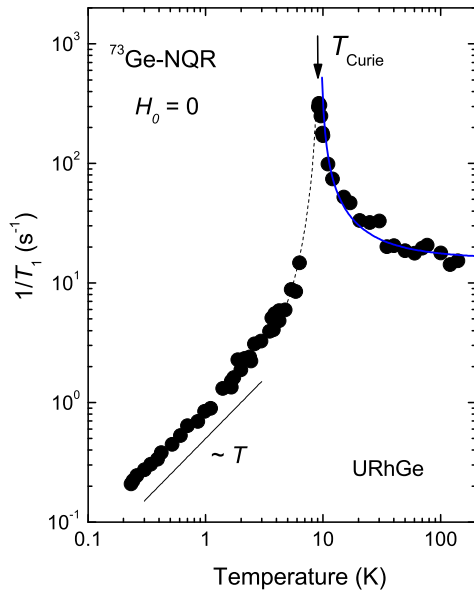


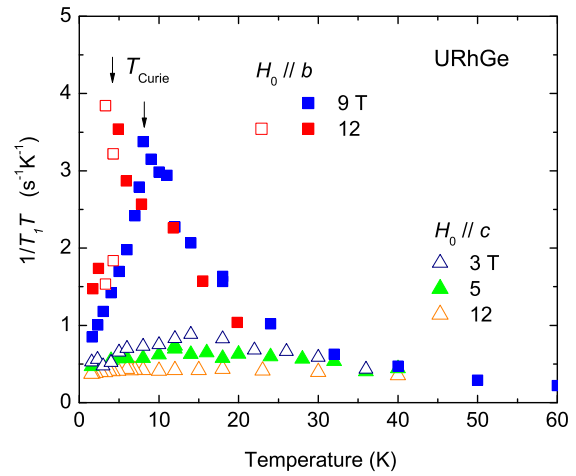
**Fig. 8.** (Color online) Temperature dependence of  $1/T_1$  measured at zero field for URhGe. The blue curve shows  $1/T_1 \propto T/(T - T_{\text{Curie}})$  expected in a three-dimensional itinerant ferromagnet.

the oriented sample is difficult, the average misalignment in this setting is expected to be  $2\text{--}3^\circ$ .

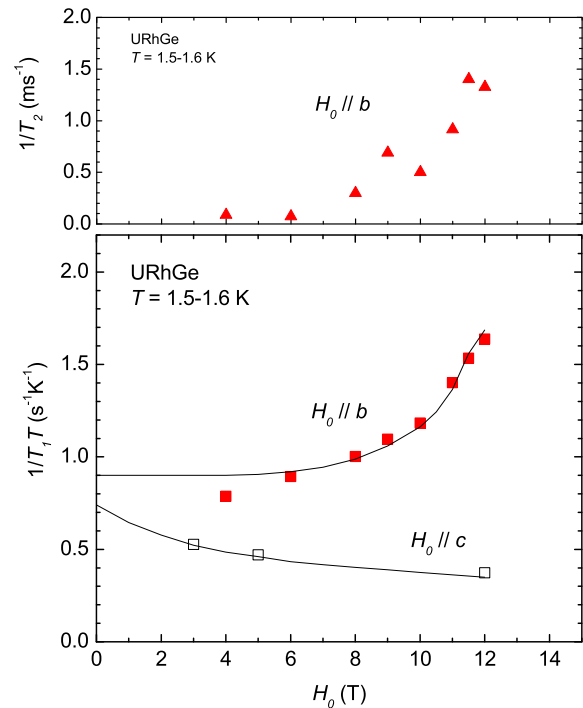
### 3.3 Temperature dependences of nuclear spin–lattice relaxation

Figure 8 shows the temperature dependence of  $1/T_1$  measured at zero field for URhGe. With decreasing temperature,  $1/T_1$  shows a divergent behavior toward  $T_{\text{Curie}}$ , followed by a gradual decrease below  $T_{\text{Curie}}$  because of a gap opening in the magnetic excitation.  $1/T_1$  well below  $T_{\text{Curie}}$  shows a  $T_1 T = \text{const.}$  behavior, which is the same as the cases in the FM1 phase of  $\text{UGe}_2$  (for example, 1.2 GPa) and in  $\text{UCoGe}$ .<sup>8,11</sup> In the PM state for URhGe,  $1/T_1$  obeys  $1/T_1 \propto T/(T - T_{\text{Curie}})$ , which is expected in a three-dimensional itinerant ferromagnet.<sup>22</sup> The itinerant character of  $f$  electrons has been confirmed by angle-resolved photoelectron spectroscopy, although the measurements have been limited below 20 K.<sup>23</sup> The behavior in  $1/T_1$  in the PM state differs from that in  $\text{UCoGe}$ ,<sup>11</sup> where  $1/T_1$  shows a gradual decrease below  $T^* \sim 40$  K. This  $T^*$  has been interpreted as a characteristic temperature, below which the itinerant character of the  $5f$  electrons is enhanced. It is conjectured that this difference between the materials originates from the difference in the band structures, and a similar difference is observed in the susceptibility measurements, where the susceptibility maximum is observed at  $\sim 40$  K for  $\text{UCoGe}$ , whereas such behavior is not observed in URhGe.<sup>24</sup>

Figure 9 shows the temperature dependence of  $1/T_1 T$  under different magnetic fields. For  $H_0 \parallel c$ ,  $1/T_1 T$  has a broad maximum at  $\sim 14$  K at  $H_0 = 3$  T, and the peak is smeared out under higher magnetic fields. The peak  $\sim 14$  K at  $H_0 = 3$  T is in good agreement with the crossover temperature, below which the NMR shift increases steeply, as shown in Fig. 4. The broadened anomaly in  $1/T_1 T$  suggests that the magnetic fluctuations are suppressed by the magnetic field along the easy axis, even for 3 T. In the case of  $H_0 \parallel b$ , on the other hand, the magnetic fluctuations remain strongly



**Fig. 9.** (Color online) Temperature dependences of  $1/T_1 T$  under different magnetic fields,  $H_0 \parallel c$  and  $H_0 \parallel b$ . For  $H_0 \parallel c$ ,  $1/T_1 T$  shows the broad peak at the crossover temperature. In contrast,  $1/T_1 T$  for  $H_0 \parallel b$  shows sharp peaks at  $T_{\text{Curie}}$ . At  $H_0 = 12$  T,  $1/T_1 T$ 's shown by the open symbols indicate those measured at the phase-separated PM and FM states.



**Fig. 10.** (Color online) Temperature dependences of  $1/T_1 T$  and  $1/T_2$ .  $1/T_1 T$  for  $H_0 \parallel b$  corresponds to the magnetic fluctuations along the  $ac$  plane and  $1/T_2$  for  $H_0 \parallel b$  corresponds to the magnetic fluctuations along the  $b$ -axis. The increases in both  $1/T_1 T$  and  $1/T_2$  toward  $H_R$  indicate that the magnetic fluctuations along the  $b$ - and  $c$ -axes are enhanced at around the spin reorientation. The curves indicate  $c_1 \gamma_5^2(H)$  (see text).

under the magnetic field.  $1/T_1 T$  at 9 T shows a sharp peak at  $\sim 8$  K, which is consistent with  $T_{\text{Curie}} \sim 7\text{--}8$  K estimated from the NMR shift shown in Fig. 6. At 12 T,  $1/T_1 T$  continues to increase in the PM state, and it is suppressed in the FM state through the phase-separation region.

### 3.4 Field dependences of nuclear spin–lattice relaxation and nuclear spin–spin relaxation

Figure 10 shows the field dependences of  $1/T_1 T$  and  $1/T_2$  at low temperatures (1.5–1.6 K).  $1/T_1 T$  for  $H_0 \parallel c$  decreases

with increasing field, whereas  $1/T_1T$  for  $H_0 \parallel b$  shows a marked increase toward 12 T, which is close to the spin-reorientation field  $H_R$ . The increase in  $1/T_1T$  under  $H_0 \parallel b$  is qualitatively consistent with the behavior in UCoGe.<sup>15)</sup> In general,  $1/T_1$  is expressed as follows:

$$\frac{1}{T_1} = \frac{\gamma_N^2}{2} \int_{-\infty}^{\infty} \langle \delta H^-(t) \delta H^+(0) \rangle \exp(-i\omega_N t) dt. \quad (1)$$

Here,  $\langle \delta H^-(t) \delta H^+(0) \rangle$  is a time correlation function for magnetic fluctuations perpendicular to the quantum axis of the nuclear spin, and  $\omega_N$  is the resonance frequency. Thus,  $1/T_1$  corresponds to the magnetic fluctuations perpendicular to the external magnetic field. Another expression for  $1/T_1T$  measured under the magnetic field along the  $\alpha$ -axis is as follows:

$$\left( \frac{1}{T_1T} \right)_\alpha = \frac{\gamma_N^2 k_B}{\gamma_e^2 \hbar^2} \sum_q \left[ A_\beta^2 \frac{\chi''_\beta(q, \omega_N)}{\omega_N} + A_\gamma^2 \frac{\chi''_\gamma(q, \omega_N)}{\omega_N} \right]. \quad (2)$$

Here,  $\chi''_\beta(q, \omega_N)$  [ $\chi''_\gamma(q, \omega_N)$ ] are imaginary parts of dynamical susceptibility along the  $\beta$  ( $\gamma$ )-axes, which are at right angles to  $\alpha$ . The difference in  $1/T_1T$  between  $H_0 \parallel b$  and  $H_0 \parallel c$  is explained by the anisotropy of the magnetic fluctuations as discussed in the case of UCoGe;<sup>12,13)</sup> however, we should discuss the anisotropy of the magnetic fluctuations using the extrapolation values toward  $H_0 \rightarrow 0$ , because the field dependences of  $1/T_1T$  are present in opposite manner between  $H_0 \parallel b$  and  $H_0 \parallel c$ .

To determine the extrapolation values toward  $H_0 \rightarrow 0$ , we show referential curves represented by  $c_i \gamma_S^2(H)$ , where  $\gamma_S(H)$  is the Sommerfeld coefficient derived from the magnetization data using the Maxwell relation,<sup>18)</sup> and  $c_i$  ( $i = a, b$ , and  $c$ ) are field-independent arbitrary parameters. This relation is based on an assumption that  $1/T_1T$  is proportional to the square of the density of states at the Fermi level, or the square of the effective mass.  $c_i$  actually depends on the hyperfine coupling constant and the anisotropy of the magnetic fluctuations. The curves of  $c_i \gamma_S^2(H)$  almost reproduce the field dependence of  $1/T_1T$  for both fields, and indicate that  $1/T_1T$  for  $H_0 \parallel c$  gradually recovers toward  $H_0 \rightarrow 0$ , whereas  $1/T_1T$  for  $H_0 \parallel b$  approaches a constant value in lower fields. The extrapolation value at  $H_0 \rightarrow 0$  is expected to be somewhat larger in  $H_0 \parallel b$ . This difference in  $1/T_1T$  corresponds to the difference between  $\chi''_b(q, \omega_N)$  and  $\chi''_c(q, \omega_N)$  from Eq. (2), because the hyperfine coupling constants are almost the same between  $H_0 \parallel b$  and  $H_0 \parallel c$ .

In UCoGe, a large difference of  $\sim 10$  times has been observed between  $1/T_1T$  for  $H_0 \parallel b$  and that for  $H_0 \parallel c$ , which is indicative of the strong Ising character of the magnetic fluctuations.<sup>12,13)</sup> Such a large difference is not observed in URhGe. We should pay attention to the fact that  $1/T_1T$  for  $H_0 \parallel b$  is very sensitive to the field along the  $c$ -axis induced by the misalignment in UCoGe.<sup>13)</sup> Actually, the coefficient  $A$  in resistivity is suppressed markedly by the low magnetic field along the  $c$ -axis.<sup>6)</sup> Using the relation of  $\gamma_S \propto \sqrt{A}$ , the initial slope near zero field in the reduction of  $\gamma_S$  is estimated to be  $d[(\gamma_S(H) - \gamma_S(0))/\gamma_S(0)]/dH \sim -30\%/T$  in UCoGe. In URhGe,  $d[(\gamma_S(H) - \gamma_S(0))/\gamma_S(0)]/dH \sim -7\%/T$  is estimated for  $H_0 \parallel c$ .<sup>18)</sup> Thus, we consider that the sensitivity in  $1/T_1T$  to the misalignment from the  $b$ -axis is not very strong in URhGe as that in UCoGe in the case at low fields. In URhGe, the small anisotropy in  $1/T_1T$  at low fields

and low temperatures suggests that the Ising character of the magnetic fluctuations well below  $T_{\text{Curie}}$  is not as strong as that in UCoGe, although a future confirmation using a single crystal is desired. The importance of the longitudinal magnetic fluctuation for superconductivity has been suggested in UCoGe.<sup>13)</sup> The weaker Ising character of the magnetic fluctuations below  $T_{\text{Curie}}$  in URhGe is likely to be relevant to induce the difference in  $T_{\text{sc}}$  between UCoGe ( $T_{\text{sc}} = 0.6$  K) and URhGe ( $T_{\text{sc}} = 0.25$  K).

Next, we discuss the magnetic fluctuation at around  $H_R$ . For  $H_0 \parallel b$ ,  $1/T_1T$  increases toward  $H_R$ . This  $1/T_1T$  corresponds to the magnetic fluctuations along both the  $a$ - and  $c$ -axes, but it is considered that the contribution along the  $c$ -axis is dominant, because the susceptibility along the  $a$ -axis is small in URhGe.<sup>18,24)</sup> On the other hand, we observed that  $1/T_2$  also increases significantly toward  $H_R$ . In general,  $1/T_2$  is expressed as follows:

$$\frac{1}{T_2} = \frac{1}{2T_1} + \lim_{\omega \rightarrow 0} \frac{\gamma_N^2}{2} \int_{-\infty}^{\infty} \langle \delta H^z(t) \delta H^z(0) \rangle \exp(-i\omega t) dt. \quad (3)$$

Here,  $\langle \delta H^z(t) \delta H^z(0) \rangle$  is the time correlation function for magnetic fluctuations parallel to the quantum axis of the nuclear spin. Thus,  $1/T_2$  corresponds to the magnetic fluctuations along the external magnetic field, that is, along the  $b$ -axis. The large enhancement of  $1/T_2$  toward  $H_R$  indicates that the magnetic fluctuations along the  $b$ -axis are enhanced, in addition to the enhancement of the magnetic fluctuations along the  $c$ -axis detected by  $1/T_1T$ . We cannot determine which of the fluctuations along the  $b$ - and  $c$ -axes is stronger, because quantitative evaluation for  $1/T_2$  is difficult.

As shown in Fig. 9, the temperature dependence of  $1/T_1T$  shows a large increase toward low temperatures in the PM phase at 12 T, where the magnetic moment is expected to lie along the  $b$ -axis. Thus, it is clear that the magnetic fluctuations perpendicular to the magnetic moment (transverse fluctuation) develop at around  $H_R$ . This is in sharp contrast to the strong-Ising case in a metamagnetic transition of UCoAl, where a critical endpoint of the metamagnetic transition is induced at a finite temperature by a magnetic field along the  $c$ -axis (easy axis). In UCoAl, the magnetic fluctuations are observed in  $1/T_2$ , whereas they are not detected in  $1/T_1T$ , when the magnetic field is applied along the  $c$ -axis.<sup>25,26)</sup> The contrasting behavior between  $1/T_1T$  and  $1/T_2$  indicates that the magnetic fluctuation has strong Ising anisotropy in UCoAl. In URhGe, magnetic fluctuations are observed in both  $1/T_2$  and  $1/T_1T$ . This indicates that the magnetic fluctuations at around  $H_R$  include both components along the  $b$ - and  $c$ -axes, and are not of strong Ising type. Theoretically, the two SC phases in URhGe have been reproduced by considering the coupling between electrons and softened magnon with transverse fluctuations.<sup>27)</sup> It is important to determine which of the fluctuations along the  $b$ - and  $c$ -axes is more crucial for the field-induced superconductivity in URhGe.

#### 4. Conclusions

We have performed  $^{73}\text{Ge}$ -NMR and NQR measurements for URhGe. Two oriented samples allowed us to investigate the static and dynamical magnetic properties of URhGe for  $H_0 \parallel c$  (easy axis) and  $H_0 \parallel b$ . The observation of the phase separation for  $H_0 \parallel b$  indicates that the spin reorientation is

of first order at low temperatures. The tricritical point was roughly estimated to be present between (10 T, 7 K) and (12 T, 4 K) on the field–temperature phase diagram for  $H_0 \parallel b$ . The nuclear spin relaxation rate  $1/T_1$  shows that the magnetic fluctuations were suppressed for  $H_0 \parallel c$ , whereas the fluctuations remain strongly under the magnetic field along the  $b$ -axis. The extrapolation values toward  $H_0 \rightarrow 0$  are likely to suggest that the Ising character of the magnetic fluctuations well below  $T_{\text{Curie}}$  in URhGe is not as strong as that in UCoGe. Toward the spin reorientation field for  $H_0 \parallel b$ , the enhancements of  $1/T_1T$  and the nuclear spin–spin relaxation rate  $1/T_2$  were observed. These indicate that the magnetic fluctuations along the  $b$ - and  $c$ -axes develop at around the first-order spin reorientation, which are the driving forces of the field-induced superconductivity in URhGe.

### Acknowledgements

We acknowledge H. Mukuda for experimental support, and D. Aoki, I. Sheikin, and K. Hattori for valuable discussions. This work was partly supported by Grants-in-Aid for Scientific Research (Nos. 24340085 and 26400359) from the Ministry of Education, Culture, Sports, Science and Technology of Japan (MEXT).

\*kotegawa@crystal.kobe-u.ac.jp

- 1) S. S. Saxena, P. Agarwal, K. Ahilan, F. M. Grosche, R. K. W. Haselwimmer, M. J. Steiner, E. Pugh, I. R. Walker, S. R. Julian, P. Monthoux, G. G. Lonzarich, A. Huxley, I. Sheikin, D. Braithwaite, and J. Flouquet, *Nature (London)* **406**, 587 (2000).
- 2) D. Aoki, A. Huxley, E. Ressouche, D. Braithwaite, J. Flouquet, J.-P. Brison, E. Lhotel, and C. Paulsen, *Nature (London)* **413**, 613 (2001).
- 3) N. T. Huy, A. Gasparini, D. E. de Nijs, Y. Huang, J. C. P. Klaasse, T. Gortenmulder, A. de Visser, A. Hamann, T. Görlach, and H. v. Löhneysen, *Phys. Rev. Lett.* **99**, 067006 (2007).
- 4) T. Akazawa, H. Hidaka, T. Fujiwara, T. C. Kobayashi, E. Yamamoto, Y. Haga, R. Settai, and Y. Ōnuki, *J. Phys.: Condens. Matter* **16**, L29 (2004).
- 5) F. Lévy, I. Sheikin, B. Grenier, and A. D. Huxley, *Science* **309**, 1343 (2005).
- 6) D. Aoki, T. D. Matsuda, V. Taufour, E. Hassinger, G. Knebel, and J. Flouquet, *J. Phys. Soc. Jpn.* **78**, 113709 (2009).
- 7) A. Huxley, I. Sheikin, E. Ressouche, N. Kernavanois, D. Braithwaite, R. Calemczuk, and J. Flouquet, *Phys. Rev. B* **63**, 144519 (2001).
- 8) H. Kotegawa, A. Harada, S. Kawasaki, Y. Kawasaki, Y. Kitaoka, Y. Haga, E. Yamamoto, Y. Ōnuki, K. M. Itoh, E. E. Haller, and H. Harima, *J. Phys. Soc. Jpn.* **74**, 705 (2005).
- 9) A. Harada, S. Kawasaki, H. Kotegawa, Y. Kitaoka, Y. Haga, E. Yamamoto, Y. Ōnuki, K. M. Itoh, E. E. Haller, and H. Harima, *J. Phys. Soc. Jpn.* **74**, 2675 (2005).
- 10) A. Harada, S. Kawasaki, H. Mukuda, Y. Kitaoka, Y. Haga, E. Yamamoto, Y. Ōnuki, K. M. Itoh, E. E. Haller, and H. Harima, *Phys. Rev. B* **75**, 140502(R) (2007).
- 11) T. Ohta, T. Hattori, K. Ishida, Y. Nakai, E. Osaki, K. Deguchi, N. K. Sato, and I. Satoh, *J. Phys. Soc. Jpn.* **79**, 023707 (2010).
- 12) Y. Ihara, T. Hattori, K. Ishida, Y. Nakai, E. Osaki, K. Deguchi, N. K. Sato, and I. Satoh, *Phys. Rev. Lett.* **105**, 206403 (2010).
- 13) T. Hattori, Y. Ihara, Y. Nakai, K. Ishida, Y. Tada, S. Fujimoto, N. Kawakami, E. Osaki, K. Deguchi, N. K. Sato, and I. Satoh, *Phys. Rev. Lett.* **108**, 066403 (2012).
- 14) T. Hattori, K. Karube, Y. Ihara, K. Ishida, K. Deguchi, N. K. Sato, and T. Yamamura, *Phys. Rev. B* **88**, 085127 (2013).
- 15) T. Hattori, K. Karube, K. Ishida, K. Deguchi, N. K. Sato, and T. Yamamura, *J. Phys. Soc. Jpn.* **83**, 073708 (2014).
- 16) A. Miyake, D. Aoki, and J. Flouquet, *J. Phys. Soc. Jpn.* **77**, 094709 (2008).
- 17) In the calculation,  $V_{zz}$  was estimated to be tilted by  $24^\circ$  from the  $a$ -axis to the  $c$ -axis, but we did not use this angle in the analysis of the spectrum. The calculation also provides  $\nu_Q^{\text{cal}} = 1.32$  MHz and  $\eta^{\text{cal}} = 0.24$ .
- 18) F. Hardy, D. Aoki, C. Meingast, P. Schweiss, P. Burger, H. v. Löhneysen, and J. Flouquet, *Phys. Rev. B* **83**, 195107 (2011).
- 19) E. A. Yelland, J. M. Barraclough, W. Wang, K. V. Kamenev, and A. D. Huxley, *Nat. Phys.* **7**, 890 (2011).
- 20) D. Aoki, G. Knebel, and J. Flouquet, *J. Phys. Soc. Jpn.* **83**, 094719 (2014).
- 21) V. P. Mineev, *Phys. Rev. B* **91**, 014506 (2015).
- 22) T. Moriya and K. Ueda, *Solid State Commun.* **15**, 169 (1974).
- 23) S. Fujimori, I. Kawasaki, A. Yasui, Y. Takeda, T. Okane, Y. Saitoh, A. Fujimori, H. Yamagami, Y. Haga, E. Yamamoto, and Y. Ōnuki, *Phys. Rev. B* **89**, 104518 (2014).
- 24) W. Knafo, T. D. Matsuda, D. Aoki, F. Hardy, G. W. Scheerer, G. Ballon, M. Nardone, A. Zitouni, C. Meingast, and J. Flouquet, *Phys. Rev. B* **86**, 184416 (2012).
- 25) H. Nohara, H. Kotegawa, H. Tou, T. D. Matsuda, E. Yamamoto, Y. Haga, Z. Fisk, Y. Ōnuki, D. Aoki, and J. Flouquet, *J. Phys. Soc. Jpn.* **80**, 093707 (2011).
- 26) K. Karube, T. Hattori, S. Kitagawa, K. Ishida, N. Kimura, and T. Komatsubara, *Phys. Rev. B* **86**, 024428 (2012).
- 27) K. Hattori and H. Tsunetsugu, *Phys. Rev. B* **87**, 064501 (2013).